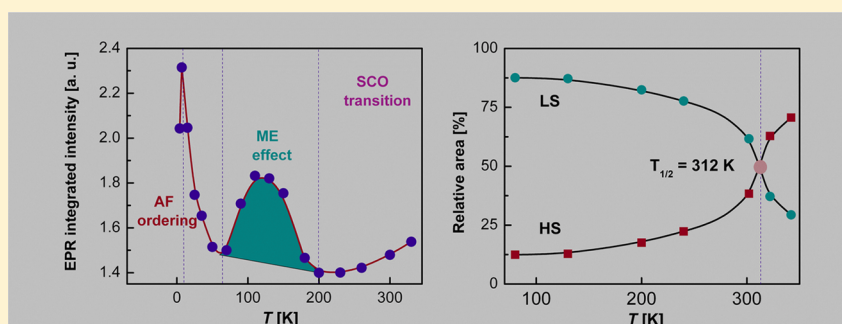


Detailed EPR Study of Spin Crossover Dendrimeric Iron(III) Complex

Natalia E. Domracheva,^{*,†} Andrew V. Pyataev,[‡] Valerya E. Vorobeva,[†] and Ekaterina M. Zueva[§][†]Zavoisky Kazan Physical-Technical Institute, Russian Academy of Science, Sibirsky Tract 10/7, 420029 Kazan, Russia[‡]Kazan Federal University, Kremlyovskaya St. 18, 420008 Kazan, Russia[§]Kazan State Technological Institute, K. Marx Street 68, 42015 Kazan, Russia

S Supporting Information



ABSTRACT: The unusual magnetic behavior of the first dendritic Fe³⁺ complex with general formula [Fe(L)₂]⁺Cl[−]·H₂O based on a branched Schiff base has been investigated by electron paramagnetic resonance (EPR) and Mössbauer spectroscopy. EPR displays that complex consists of the three types of magnetically active iron centers: one *S* = 1/2 low-spin (LS) and two *S* = 5/2 high-spin (HS) centers with strong low-symmetry and weak distorted octahedral crystal fields. Analysis of the magnetic behavior reflected by *I* versus *T* (where *I* is the EPR lines integrated intensity of the spectrum) demonstrates that the dendritic Fe³⁺ complex has sufficiently different behavior in three temperature intervals. The first (4.2–50 K) interval corresponds to the antiferromagnetic exchange interactions between LS–LS, LS–HS, and HS–HS centers. The appearance of a presumable magnetoelectric effect is registered in the second (50–200 K) temperature interval, whereas a spin transition process between LS and HS centers occurs in the third (200–330 K) one. The coexistence of the magnetic ordering, presumable magnetoelectric effect, and spin crossover in one and the same material has been detected for the first time. The Mössbauer spectroscopy data completely confirm the EPR results.

■ INTRODUCTION

Dendritic materials are interesting due to their unique macromolecular monodispersed nature and generation-dependent properties.^{1,2} Dendrimers are regularly branched compounds provided with a defined number of end groups, whose modification allows one to “fine tune” their properties. Such materials have received much attention recently with regard to fundamental research and because of their applications in various fields.^{3–5} Incorporation of transition metals in dendrimer leads to new and interesting compounds with specific properties, such as the capability to absorb visible light, to exhibit luminescence, and to undergo reversible multi-electron redox processes.^{6,7} These materials may find applications as components in molecular electronics and as photochemical molecular devices for solar energy conversion and information storage.⁶

The motivation of this work is to make a hybrid material that would combine the properties of dendrimer with the unusual magnetic transition metal properties such as spin crossover (SCO) behavior. Transition metal complexes with SCO behavior have been extensively studied in the last seven decades.⁸ Their unique magnetic behavior is very useful for

various applications such as display devices, optical switches, and magneto-optical storage systems.^{8–10} Iron centers in SCO complexes can adopt two different spin states that are transferred from low-spin (LS) to high-spin (HS) states upon external perturbations⁹ like heat, light, pressure, and magnetic fields or by chemical alteration (ligand substitution, nature of anion, and crystal solvent).

The first step in creating such a hybrid material was accomplished by Fujigaya¹¹ who presented spin-crossover iron(II) complexes with triazole-based dendritic ligands. Synthesized compounds were magnetically active, and their spin-transition profiles were highly dependent on the generation number of the dendritic unit. Fujigaya's study clearly indicates that dendrimers are useful components for functional soft materials. However, conversion from low to high spin states in his compounds was irreversible due to irreversible loss of water molecule during the first heating process leading to the spin change. Stimulated by this experiment, the scientific

Received: April 15, 2013

Revised: June 4, 2013

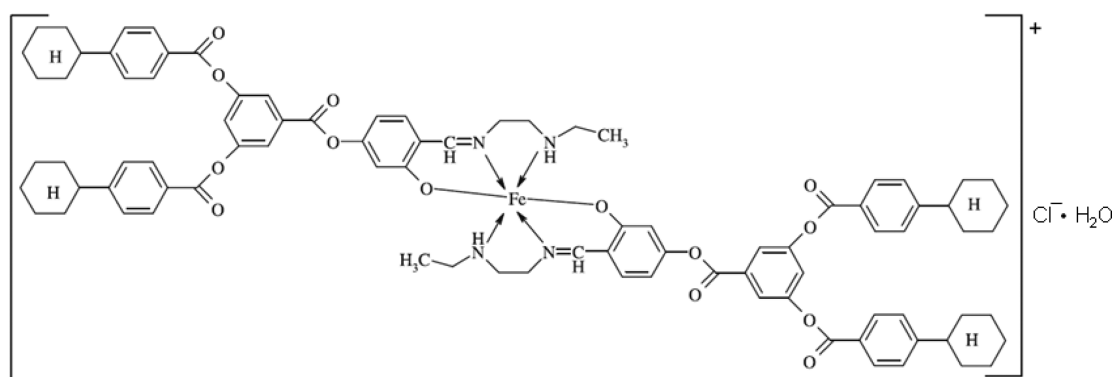


Figure 1. Schematic model of the compound.

group headed by Gutlich^{12,13} tried to find dendritic triazole-based complexes with reversible spin-transition. All their dendritic iron(II) compounds displayed spin-transition behavior that depended on the coordinated water molecules present in the iron(II) complex. Spin-state conversion was triggered by thermally induced water release, and a gradual spin transition took place after the first heat treatment to 350 K. It has also been shown that the nature of the counteranions and the type of dendritic ligands play an important role for the magnetic behavior, which is reflected by $\chi_M T$ versus T .

It is known, however, that suitability of the material for practical applications¹⁴ depends strongly on its chemical stability. This aspect is particularly important in the case of iron(II) complexes due to their tendency to be oxidized more or less easily in ambient atmosphere. That is why we direct our attention to dendritic systems based on SCO iron(III) complexes which are noted by their chemical stability. Fe³⁺ compounds^{15,16} exhibit also spin-crossover behavior, and it is related to electronic transition between t_{2g}^5 [low spin (LS)] and $t_{2g}^3 e_g^2$ [high spin (HS)] states. The situation is similar to Fe(II) compounds, the difference being in the spin multiplicity of the LS and HS states: for iron(III), these being a doublet 2T_2 , $S = 1/2$, and a sextet 6A_1 , $S = 5/2$, respectively. SCO Fe³⁺ complexes may be classified into two groups depending on the spin transition profile: (i) spin transition (ST) type, the spin transition between HS and LS states occurs abruptly within a few Kelvin; (ii) spin equilibrium (SE) type, the spin transition occurs gradually over a wide temperature range.

According to what was mentioned above, we decided to make a spin-crossover dendrimeric Fe³⁺ system where the Fe³⁺ complex with Schiff-base ligands would play the role of a central SCO magnetic block surrounded by the branched dendrimeric structure. The syntheses and characterization of such spin-crossover dendrimeric Fe³⁺ systems have been reported in our previous publication.¹⁷ It has been shown¹⁷ that the compound is a monocationic bis(ligand) Fe³⁺ complex $[\text{Fe}(\text{L})_2]^+ \text{Cl}^- \cdot \text{H}_2\text{O}$, where iron(III) ion has an octahedral geometry with N_4O_2 donor atoms formed by three ligand (ONN) atoms of tridentate ligand (L). The elemental analysis and mass-spectrometry data permit one to construct a schematic model of the complex, which is given in Figure 1.

In this work, we have focused our attention on a detailed study of the spin transition features in this new system using EPR and Mössbauer spectroscopy. DFT calculations have also been used to determine the coordination sphere structure of the compound.

EXPERIMENTAL SECTION

Synthesis and Characterization of Material. The synthesis of the bis-chelate Fe³⁺ complex based on 3,5-di(4-cyclohexylbenzoyloxy)benzoyl-4-oxysalicylidene-*N'*-ethyl-*N*-ethylenediamine with a chlorine counterion and its characterization by elemental analysis, infrared (IR), NMR, and EPR spectroscopy, the MALDI-ToF-MS method, and DSC calorimetry are described in ref 17.

Physical Measurements. EPR studies were performed using a CW-EPR EMXplus Bruker spectrometer operating at 9.41 GHz (X-band); the modulation frequency was 100 kHz. Commercial cryostats were used to vary the temperature of a sample in the range 4.2–330 K. All Mössbauer spectra were obtained using a conventional constant-acceleration spectrometer where ⁵⁷Co in Rh matrix was used as the source. The velocity calibration was obtained by using the α -Fe spectrum. The isomer shift data were reported relative to the isomer shift of the α -Fe spectrum. A liquid nitrogen continuous-flow cryostat was used for the temperature measurements in the range 80–302 K. The lower temperature measurements were made using a helium cryostat. The Mössbauer absorber, which was prepared as a thin layer of powder between two aluminum foil discs, was mounted on the copper sample holder of the helium cryostat. The higher temperature measurements were made using a Mössbauer furnace. The temperature measurements and control were carried out by a type-T thermocouple and a heater above 50 K with an accuracy of 0.2 K. A carbon-resistance thermometer, calibrated at the liquid nitrogen and liquid helium temperatures, was used for the temperature measurements and control below 50 K with an accuracy of 0.5 K.

DFT Calculations. Geometry optimizations were performed within the PBE framework^{18,19} using the so-called 3z basis set²⁰ of TZ2P quality (PRIRODA, version 5.0²¹ package), whereas the *g*-factors were calculated using the B3LYP functional²² in conjunction with the CP(PPP) basis set²³ for iron atoms and TZVP²⁴ for the remaining atoms (ORCA, version 2.8²⁵ package). All ORCA calculations were performed with the increased integration grid (Grid4). For the iron atoms, an enhanced integration grid was employed and the overall integration accuracy was increased to 7.0.

RESULTS AND DISCUSSION

Electron Paramagnetic Resonance Spectroscopy. EPR is a powerful technique for observing spin transition and studying spin dynamics in Fe³⁺ complexes.^{26–32} This method allows not only a confirmation of the existence of LS and HS

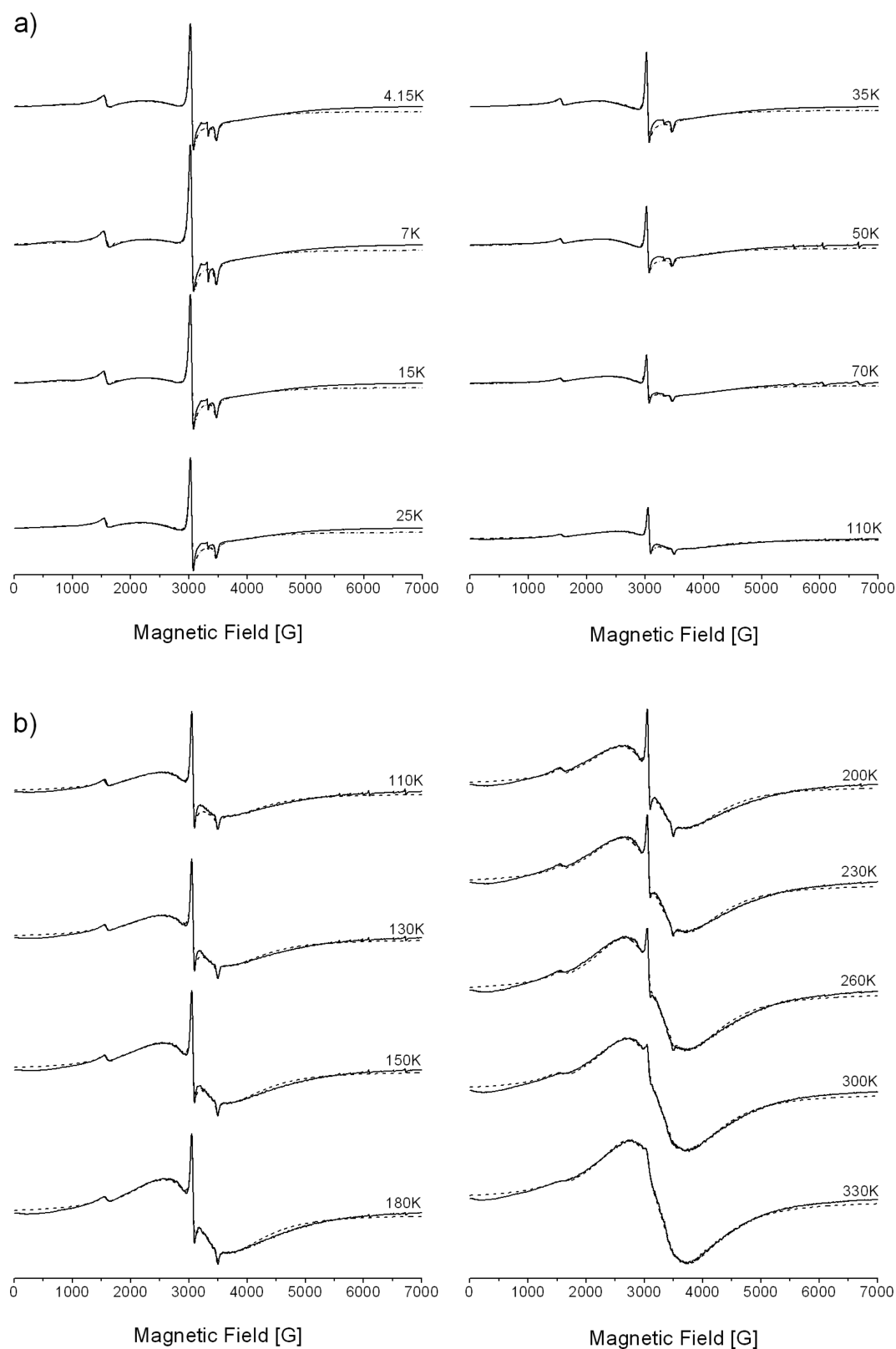


Figure 2. The temperature dependence of the EPR spectra of the compound from (a) 4.15 to 110 K and (b) 110 to 330 K. Spectra in the temperature range (b) are recorded at higher amplification ($\times 1.4$) in comparison with spectra in the range (a). The short dashed lines show the theoretical EPR spectra.

fractions in the compound but also an investigation of their evolution with temperature. Figure 2 shows the transformation of X-band EPR spectra ($h\nu = 0.3 \text{ cm}^{-1}$) of polycrystalline sample measured at temperatures from 4.2 to 330 K. To avoid

the influence of molecular oxygen, the sample was degassed to 10^{-3} mmHg .

As can be seen, EPR spectra demonstrate the presence in the system of three types of iron(III) centers: two types of HS ions

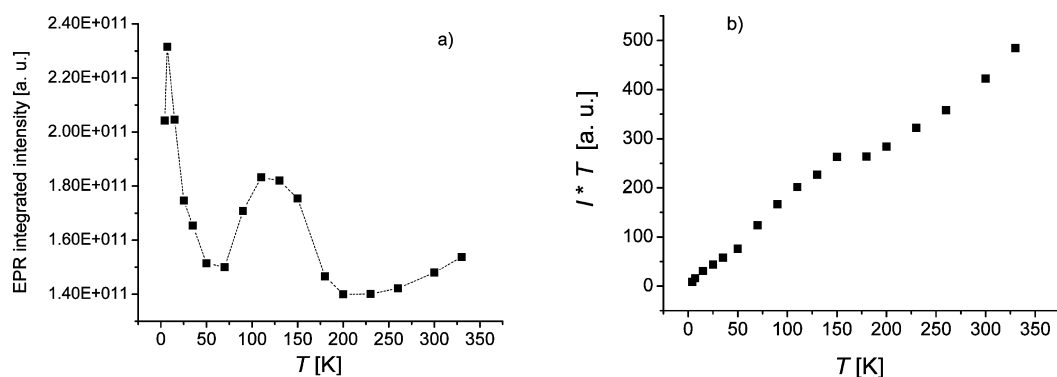


Figure 3. (a) The temperature dependence of the EPR lines integrated intensity of the whole EPR spectrum. (b) The $I \times T$ vs T plot, showing a stepwise behavior.

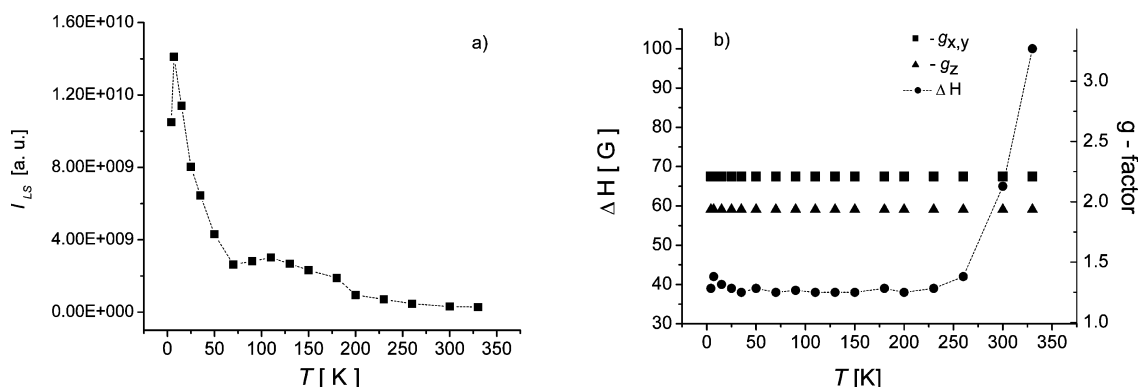


Figure 4. (a) The temperature dependence of the EPR lines integrated intensity of the LS centers. (b) The temperature dependence of the g-factor and the width of the individual lines of the LS centers.

and one of LS. The EPR spectra of HS Fe^{3+} centers (that have the ${}^6\text{A}_{1g}$ ground state) are described by the spin-Hamiltonian:^{33,34}

$$\hat{H} = g\beta\hat{B}\hat{S} + D\left[\hat{S}_z^2 - \frac{1}{3}S(S+1)\right] + E(\hat{S}_x^2 - \hat{S}_y^2) \quad (1)$$

where g is the isotropic g factor, D and E are the fine structure parameters of the EPR spectrum, $S = 5/2$, and $0 < E/D \leq 1/3$. The positions of the fine structure lines depend on the value of the ratio between the microwave quantum $h\nu$ and D parameter. Theoretical analysis shows^{33,34} that the signal with $g = 4.26$ belongs to HS iron ions with strong ($D > h\nu = 0.3 \text{ cm}^{-1}$) low-symmetry ($E/D \sim 1/3$) crystal field (I-type of HS centers), whereas the broad signal with $g \sim 2$ belongs to HS Fe^{3+} ions in an octahedral environment with weak ($D < 0.3 \text{ cm}^{-1}$, $E = 0$) distorted crystal field (II-type of HS centers).

The EPR spectra of the LS Fe^{3+} centers (that have the ${}^2\text{T}_{2g}$ ground state) are described by the spin Hamiltonian:

$$\hat{H} = \beta(g_x\hat{B}_x\hat{S}_x + g_y\hat{B}_y\hat{S}_y + g_z\hat{B}_z\hat{S}_z) \quad (2)$$

where the g -tensor values are close to 2. LS Fe^{3+} centers give an anisotropic EPR signal, and the g -tensor has an axial anisotropy: $g_x = g_y = 2.21$, $g_z = 1.935$. It should be noted that the g -values found are typical to those determined for the known LS iron(III) complexes.^{35–37}

Heating of the sample from 4.2 to 330 K is accompanied by decrease of the number of I-type HS centers and transformation of LS centers to HS centers of the II-type. The evolution of the last centers indicates the existence of the spin

($S = 1/2 \leftrightarrow 5/2$) transition process between ${}^2\text{T}_{2g}$ and ${}^6\text{A}_{1g}$ states.

The temperature dependence of the EPR lines integrated intensity (I) is one of the sources of information about the spin transition process. Note that I is obtained by numerical double integration of the EPR spectrum and it is proportional to the static paramagnetic susceptibility. The magnetic behavior of the compound reflected by the temperature dependencies of I and $I \times T$ product of the whole EPR spectrum is shown in Figure 3. One can see that the temperature dependence of I has complicated, three-step behavior: it reaches the first maximum at 7 K and then drops to a minimal value at about 50 K, reaches the second maximum at about 125 K and then drops to a minimal value at about 200 K, and further begins to grow (Figure 3a). Variation of the $I \times T$ product from temperature shows that the complex undergoes a gradual spin transition (SE-type) and has a stepwise behavior at about 50–200 K (Figure 3b). Note that all temperature dependencies in Figure 3 are fully reversible. According to the obtained data, we can denote $I(T)$ dependence by three intervals: I (4.2–50 K), II (50–200 K), and III (200–330 K) characterized by different behavior.

Let us try to understand the origin of the observed anomaly in our compound. For this purpose, the temperature dependencies of the EPR lines integrated intensity were examined for each type of Fe^{3+} centers separately. The analysis of the EPR signals for each type of Fe^{3+} centers was based on the procedure of fitting of the model spectrum to the observed experimental one. To fit the EPR spectra written in numerical

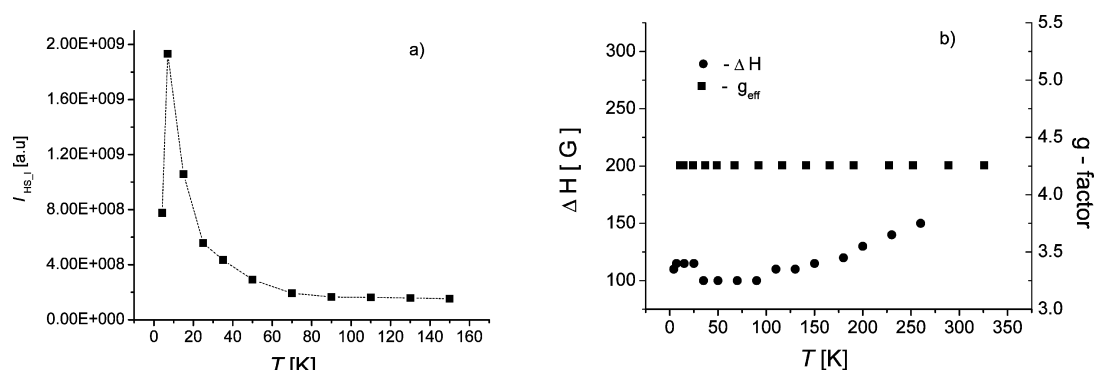


Figure 5. (a) The temperature dependence of the EPR lines integrated intensity of the I-type HS iron(III) centers. (b) The temperature dependence of the g-factor and the width of the individual line of the I-type HS iron(III) centers.

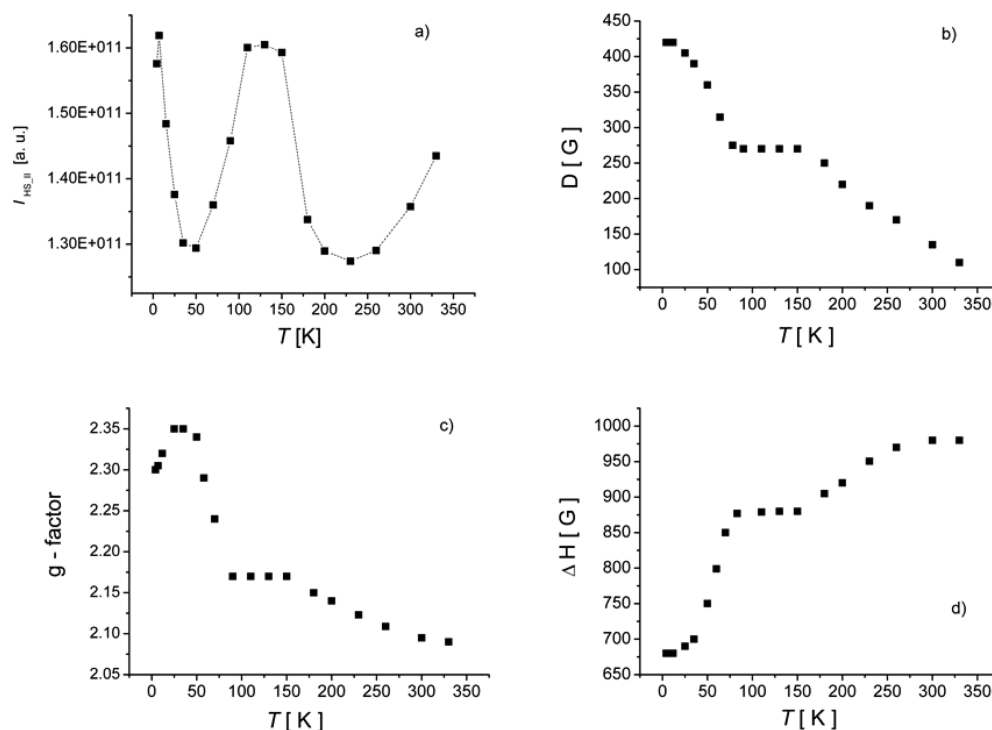


Figure 6. The temperature dependencies of the EPR lines integrated intensity (a), D parameter (b), g-factor (c), and the width of the individual lines of the II-type HS iron(III) centers (d).

format, we used the standard EasySpin-EPR spectrum simulation program. Two examples of spectra simulation are presented in the Supporting Information. The parameters of the fit were the g - and D -tensor components, the line shape, and the widths of the individual components ΔH . Simulated in this way, EPR spectra are shown in Figure 2 (see short dashed lines). As can be seen, a good agreement is obtained between the experimental and theoretical spectra.

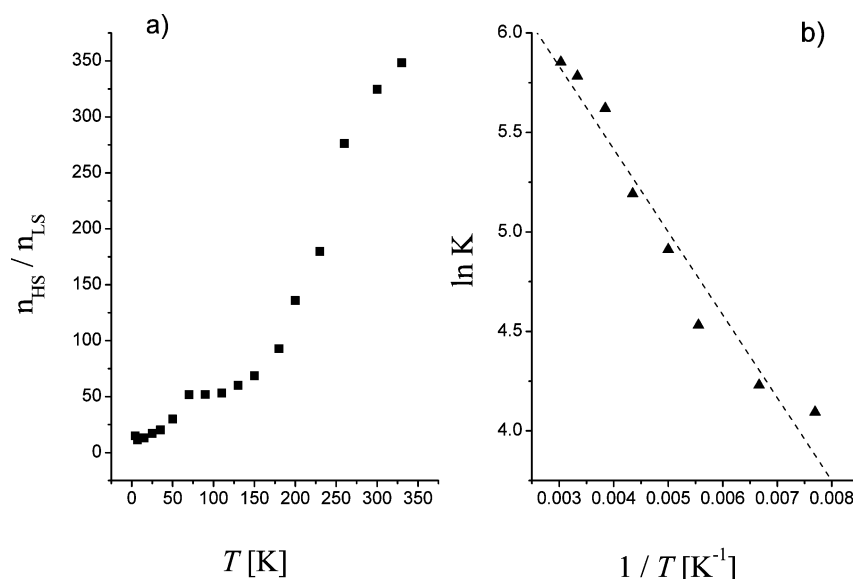
As the first step, we will turn our attention to the estimation of the fine structure parameter (D) of the broad signal belonging to HS Fe^{3+} ions of the II-type (octahedral iron centers with weak axial distortion). The theory developed for the calculation of D -parameter in HS iron(III) complexes showed that D consists of the contributions of the low lying excited quartet states mixed with the ground sextet state due to the spin–orbital coupling (SOC).³⁸ Using the obtained theoretical equation for D ,³⁸ the energy gaps between the ground-state and excited terms and SOC of Fe^{3+} ion equal $\zeta_{\text{Fe}} = 397 \text{ cm}^{-1}$. Murav'ev³⁹ on the example of similar HS iron(III)

complexes estimated that the D -parameter should be in the following range: $0.01 \text{ cm}^{-1} < |D| < 0.04 \text{ cm}^{-1}$. D values evaluated by him agree with our experimental EPR data ($g = 2.1$, $|D| = 0.043 \text{ cm}^{-1}$) obtained for the liquid-crystalline HS iron(III) complex with Schiff-based ligands.⁴⁰ Therefore, fitting the model spectra of the II-type HS Fe^{3+} ions, we used the D parameter which changed in the range $0.01\text{--}0.045 \text{ cm}^{-1}$.

Now let us analyze the EPR spectra of each type of Fe^{3+} centers independently. Figures 4, 5, and 6 show the temperature variation of the EPR integrated intensity (I), g , ΔH , and D parameter values for the LS and two types of HS centers, respectively. As can be seen, the EPR integrated intensities (I) for all three types of iron(III) centers demonstrate a maximum at $T_N = 7 \text{ K}$ in the temperature interval 4.2–50 K. The appearance of a maximum on the curves shows that the LS and HS iron centers are coupled by antiferromagnetic exchange interactions. This fact is confirmed by the Mössbauer spectroscopy data presented below. Note that a similar behavior was detected for the resembling iron(III)

Table 1. Calculated EPR Parameters of LS Fe³⁺ Centers of Complex

| LS Fe ³⁺ centers | g_x | g_y | g_z | A | B | C | k | Δ/ζ | V/ζ | $\Delta E_{12}/\zeta$ | $\Delta E_{13}/\zeta$ |
|-----------------------------|-------|-------|-------|--------|--------|-----|-------|----------------|-----------|-----------------------|-----------------------|
| | -2.21 | -2.21 | 1.935 | 0.0971 | 0.9936 | 0 | 0.867 | 2.556 | 0.00 | 7.307 | 8.238 |

Figure 7. (a) HS/LS vs T profile for a gradual SCO behavior. (b) $\ln K$ vs $1/T$ for complex.

complexes with Schiff-based ligands, where the appearance of a maximum at $T_N = 7$ K was caused by bridging iron centers by means of counteranion and water molecule.³⁷ Thus, we can assume that in our complex LS–LS, LS–HS, and HS–HS centers are coupled together, where the Cl[−] counterion and H₂O molecule play the role of bridging units.

The analysis of the EPR signal of the LS centers shows that the g_{xy} and g_z values are independent of temperature (Figure 4b) and the width of the individual lines remains practically unchanged in the temperature interval (I–II) and begins to grow after 200 K. The experimental values of g -factor were used to determine the ground state for LS Fe³⁺ centers in complex. The g -values have been analyzed within the single-electron approximation for the lower orbital triplet according to the approach described in refs 35–37. We will not stop on the explanation of this theoretical approach described in detail in our previous work³⁷ but only pass to the obtained results. The calculated parameters found by the above-mentioned theory are listed in Table 1, where the theoretical g factors, the A , B , and C coefficients of the wave functions of the ground Kramer's doublet, the k coefficient of suppression of the spin–orbit coupling, the axial (Δ) and rhombic (V) components of the crystal field, and the relative energies of the ground and two excited ΔE_{12} , ΔE_{13} Kramer's doublet are given. As seen from Table 1, the iron complex has the largest coefficient B , which indicates that the ground-state Kramer's doublet is characterized by the state where the unpaired electron resides in the d_{xy} orbital, and thus $(d_{xz}d_{yz})^4(d_{xy})^1$ is the ground state for LS Fe³⁺ centers.

The temperature dependence of I for HS centers of the I-type shows that the number of these centers monotonously decreases after 7 K (Figure 5a). It means that such HS centers do not take part in the spin transition. The g -factor of these centers is independent of temperature, and the width of the individual line only slightly grows with temperature increase (Figure 5b).

The most interesting features display HS Fe³⁺ centers of the II-type (octahedral centers with weak axial distortion). Their temperature dependence of I_{HS} reproduces the peculiarities of I for the whole EPR spectrum. The behavior of the D parameter, g -factor, and the width of the individual lines of these HS centers are shown in Figure 6b, c, and d, respectively. In order to understand the observed peculiarities and to establish the temperature range where LS \leftrightarrow HS spin transition takes place, we calculate the change in the number of HS molecules of the II-type (HS fraction) with respect to LS molecules (LS fraction) with an increase in temperature. As seen in Figure 7a, this ratio n_{HS}/n_{LS} begins to increase after 150 K up to 330 K and this behavior testifies to the spin equilibrium process between $^2T_{2g}$ and $^6A_{1g}$ states (gradual change in the spin state). The enthalpy and entropy changes accompanying the spin transition are evaluated by using eq 3:

$$\ln K = \ln(n_{HS}/n_{LS}) = -\Delta H/RT + \Delta S/R \quad (3)$$

where K is the equilibrium constant and R is the gas constant. The thermodynamic parameters—the enthalpy (ΔH) and entropy (ΔS) of the spin equilibrium process, $\Delta H = 3.46$ kJ/mol and $\Delta S = 58.88$ J·K^{−1}/mol—were calculated from the straight line given by plotting $\ln K$ versus $1/T$ (Figure 7b). The ΔH and ΔS values estimated are close to those found for other iron(III) spin-crossover complexes.^{27,41} The enthalpy changes accompanying the spin transition are 6 times as large as the values expected for the magnetic contribution of the $^6A \leftrightarrow ^2T$ process ($R \ln 3 = 9.1$ J·K^{−1}/mol). This fact shows that the lattice vibrations of a complex play an important role in the spin transition.⁴² All of these investigations permit one to affirm that a most sharp changing in the spin transition profile takes place from 200 to 330 K. This result agrees well with the Mössbauer data presented below (see Figure 9b).

At the end of this paragraph, we may conclude that the antiferromagnetic exchange interactions prevail in the first (I, 4.2–50 K) temperature interval, while the spin equilibrium

process dominates in the third (III, 200–330 K) one. The question arises: what physical phenomenon is responsible for the anomaly behavior of the EPR integrated intensity (I) in the second (II, 50–200 K) temperature interval (see Figure 3a and 6a)? We think that this anomaly is caused by the magneto-electric effect. This conclusion follows from the analogous behavior of the EPR lines integrated intensity observed in the liquid-crystalline state of the iron(III) complex.⁴⁰ It has been shown in ref 40 that the integrated intensity of Fe^{3+} EPR lines in the ferroelectric mesophase is increased (as compared to that predicted by the Curie–Weiss law), and it has an anomalous behavior at the same temperature range as the static dielectric permittivity does.⁴³ The observed anomaly arose due to action of the internal electric field (existing in the mesophase) on magnetic properties via the magnetoelectric effect.

The additional arguments for the existence of the internal electric field in our complex are the $g(T)$ and $D(T)$ dependencies of HS Fe^{III} centers of the II-type. It is well-known⁴⁴ that the electric field's effect results in the shift of the g -factor, as well as in that of the D -tensor. Figure 6b shows that, when the system transfers from HS to LS state with temperature decrease, the D parameter gradually grows. Such change of D parameter indicates the changing of the electric polarization of iron ion. A similar behavior is registered also for g -factor (Figure 6c). Thus, simultaneously with the spin equilibrium process, the changing of electric polarization takes place in our compound.

Let us dwell shortly on the theory that can predict the behavior observed. One year ago, a new view on the materials with simultaneous coexisting ferroelectric and magnetic properties (so-called multiferroics) was suggested by Bersuker.⁴⁵ In his theoretical approach, the local vibronic coupling between the ground and excited states of opposite parity, the pseudo-Jahn–Teller effect (PJTE), may lead to spontaneous displacements forming local dipole moments; their cooperative interaction results in ferroelectric phase transitions of order–disorder type. This (PJTE) theory of ferroelectricity explains well the origin of perovskite multiferroics and formulates the necessary conditions of simultaneous coexisting ferroelectric and magnetic properties. In combination with the HS–LS crossover effect, this leads to a novel phenomenon, called the magnetic–ferroelectric (multiferroics) crossover (MFCO). According to Bersuker analysis, d^5 LS and HS Fe^{3+} ions satisfy the necessary conditions of potential multiferroics. Thus, the change of the spin state for the d^5 configuration can change also the ferroelectric state and the SCO is simultaneously a magnetic–ferroelectric (multiferroics) crossover (MFCO).

The vibronic (PJTE) theory may explain our experimental results indicating the local origin of the observed effects. We suppose that our compound is the first example of magnetic–ferroelectric (multiferroics) crossover (MFCO) material.

Mössbauer Spectroscopy Study. Mössbauer spectra of the compound at various temperatures are shown in Figure 8. The spectrum recorded at 342 K consists of two doublets. One doublet with isomer shift $\delta_{\text{Fe}} = 0.2$ mm/s and quadrupole splitting $Q_S = 0.34$ mm/s refers to Fe^{3+} in the HS state. A second doublet with $\delta_{\text{Fe}} = 0.31$ mm/s and $Q_S = 0.95$ mm/s corresponds to the Fe^{3+} LS species. The calculated parameters of the HS and LS iron(III) centers at different temperatures are shown in Table 2.

Figure 9a demonstrates the temperature dependencies of the relative areas of the HS and LS fractions, whose behaviors indicate the gradual spin transition. The temperature, $T_{1/2}$, at

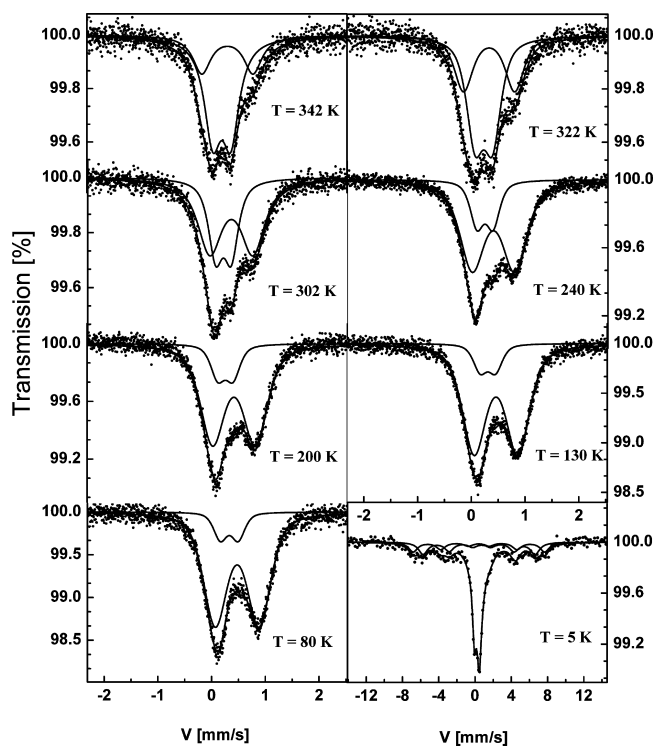


Figure 8. Mössbauer transmission spectra of the compound at various temperatures.

Table 2. Calculated Parameters of the Mössbauer Spectra for the $[\text{Fe}(\text{L})_2]^+\text{Cl}^-\cdot\text{H}_2\text{O}$ Complex

| T (K) | low-spin state | | high-spin state | | % area | |
|------------|--------------------------------|-----------------------------|--------------------------------|-----------------------------|--------|------|
| | Δ_{Fe} (mm/s) | Q_S^{LS} (mm/s) | Δ_{Fe} (mm/s) | Q_S^{HS} (mm/s) | HS | LS |
| 342 | 0.31 | 0.95 | 0.2 | 0.34 | 70.6 | 29.4 |
| 302 | 0.37 | 0.8 | 0.22 | 0.29 | 38.3 | 61.7 |
| 80 | 0.47 | 0.81 | 0.33 | 0.33 | 12.5 | 87.5 |

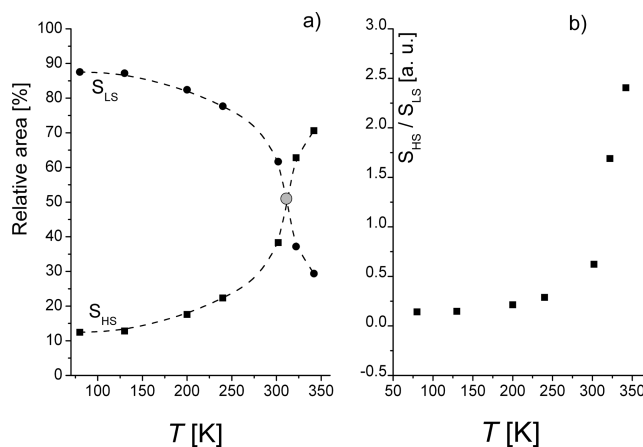
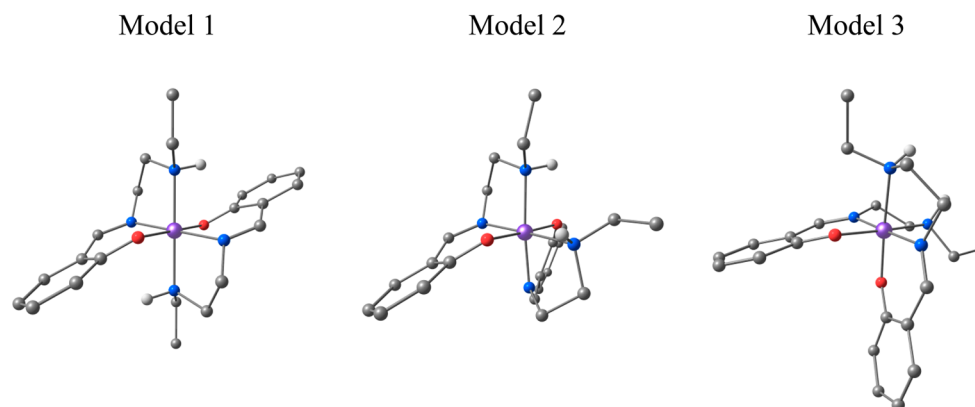


Figure 9. (a) The temperature dependence of the relative areas of HS and LS fractions (S_{HS} , S_{LS}). (b) The temperature dependence of the ($S_{\text{HS}}/S_{\text{LS}}$) ratio.

which 50% of area of centers are in the LS state is 312 ± 2 K (gray point in Figure 9a). The change in the area of HS fraction with respect to the LS one ($S_{\text{HS}}/S_{\text{LS}}$) upon temperature increase is shown in Figure 9b. One can see that the $S_{\text{HS}}/S_{\text{LS}}$ ratio begins to increase sharply after 160 K.

Chart 1. Coordination Models of the Compound^a

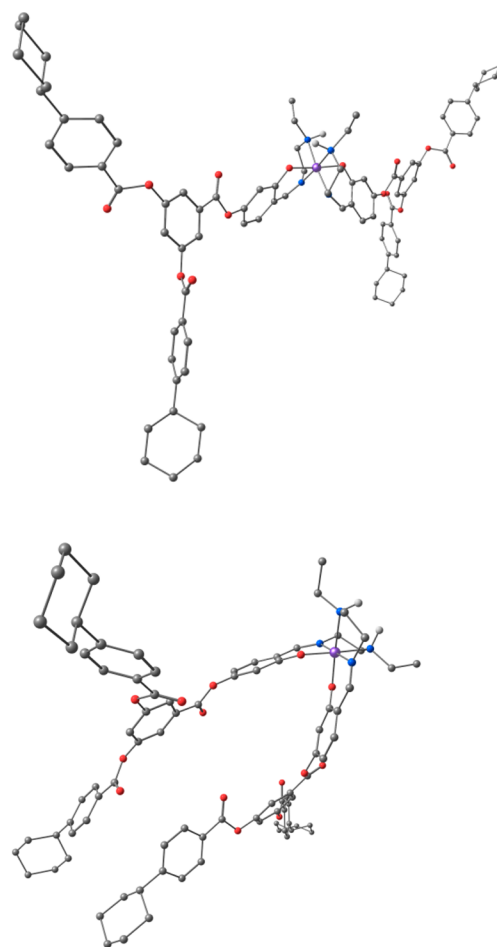
^aThe ligand tails are not shown.

The spectrum measured at 5 K detects two nonequivalent HS state positions of the ^{57}Fe atoms (Figure 8). These two Fe^{3+} HS positions give two Zeeman sextets characterized by the following parameters: the first with $\delta_{\text{Fe}} = 0.42$ mm/s, $Q_{\text{S}}^{\text{HS}} \sim 0$ mm/s, and $H_{\text{hf}} = 450$ kOe and the second one with $\delta_{\text{Fe}} = 0.59$ mm/s, $Q_{\text{S}}^{\text{HS}} = -0.29$ mm/s, and $H_{\text{hf}} = 383$ kOe. Fe^{3+} LS centers show a badly resolved magnetic hyperfine structure in the central part of the spectrum with parameters $\delta_{\text{Fe}} \sim 0.5$ mm/s, $Q_{\text{S}}^{\text{LS}} \sim 0.8$ mm/s, and $H_{\text{hf}} \sim 30$ kOe. The appearance of the hyperfine structures in the spectrum indicates the existence of the magnetic ordering in the system. That result is also consistent with the EPR data.

DFT Calculations. The spectroscopic studies do not provide unambiguous information on the coordination sphere structure of our complex. If the ligand is flexible enough, the complex can exhibit different coordination modes. In this section, on the basis of the comparison of the DFT-based g -factors (computed for different coordination models) and EPR-based ones, we assign the structure for the LS coordination core. The calculations were performed using the model complex, where the ligand tails were omitted. Indeed, several minima corresponding to different isomers (see Chart 1) were found on the LS state potential energy surface. In two of these isomers, the phenolate oxygen atoms are in a *trans*-position to each other (i.e., form the O–Fe–O axis), whereas the nitrogen atoms form either the N–Fe–N and N(H)–Fe–N(H) axes (model 1) or two N–Fe–N(H) axes (model 2). The third isomer contains the N–Fe–N axis and two O–Fe–N(H) ones (model 3). It should be noted that the ligand moiety is bent in the first two coordination models, whereas it is planar in the last one. The calculated principal values of g -tensor are [2.175, 2.073, 2.016], [2.159, 2.059, 2.022], and [2.110, 2.101, 2.031] for models 1, 2, and 3, respectively. Obviously, model 3 is the only one consistent with the EPR data. According to calculations, model 3 is also energetically most preferable (models 1 and 2 are 28.8 and 23.0 $\text{kJ}\cdot\text{mol}^{-1}$ higher in energy). The energies of the full complexes follow the same trend.

It should be stressed that only in two models (2 and 3) the N(H) donor atoms occupy the neighboring positions in the coordination polyhedron (see Chart 2). Such coordination sphere structures allow the formation of dimeric ensembles, where the iron sites are coupled by weak intermolecular interactions (H-bonds between the NRH fragments of the neighboring complexes, water molecules, and chlorine counterions), which dominate in the first (I) temperature interval. An

Chart 2. Examples of Complexes with the Neighboring N(H) Donor Atoms



example of such a possibility for a similar compound (however, with the NH_2 fragments) has been demonstrated in the literature.⁴⁶ Unfortunately, all our attempts to locate such equilibrium structures were unsuccessful. However, a critical role in their formation may play the crystal packing effects, which are not included in the calculation.

■ CONCLUSIONS

We have presented a new multifunctional material—a dendrimeric Fe³⁺ spin crossover complex exhibiting a magnetic ordering, presumable magnetoelectric effect, and thermally driven spin transition in one and the same material. This coexistence of strongly correlated magnetic, ferroelectric, and spin-crossover phenomena opens a variety of new possibilities to manipulate the properties of the system with exciting novel functionalities for electronics and spintronics.

■ ASSOCIATED CONTENT

■ Supporting Information

The simulated EPR spectra at 110 and 200 K are presented. This material is available free of charge via the Internet at <http://pubs.acs.org>.

■ AUTHOR INFORMATION

Corresponding Author

*E-mail: domracheva@mail.knc.ru; ndomracheva@gmail.com.
Phone: +7(843) 2319065.

Notes

The authors declare no competing financial interest.

■ ACKNOWLEDGMENTS

We gratefully acknowledge the financial support for this work by RAS Presidium program no. 24 and in part by the RFBR, project no. 11-03-01028. We thank M. S. Gruzdev, U. V. Chervonova, A. M. Kolker, and A. S. Golubeva for the sample presentation.

■ REFERENCES

- (1) Carlmark, A.; Hawker, C.; Hult, A.; Malkoch, M. New Methodologies in the Construction of Dendritic Materials. *Chem. Soc. Rev.* **2009**, *38*, 352–362.
- (2) Frauenrath, H. Dendronized Polymers—Building a New Bridge from Molecules to Nanoscopic Objects. *Prog. Polym. Sci.* **2005**, *30*, 325–384.
- (3) Zeng, F.; Zimmerman, S. C. Dendrimers in Supramolecular Chemistry: From Molecular Recognition to Self-Assembly. *Chem. Rev.* **1997**, *97*, 1681–1712.
- (4) Diaz, D. J.; Storrer, G. D.; Bernhard, S.; Takada, K.; Abruna, H. D. Ordered Arrays Generated via Metal-Initiated Self-Assembly of Terpyridine Containing Dendrimers and Bridging Ligands. *Langmuir* **1999**, *15*, 7351–7354.
- (5) (a) Newkome, G. R.; Moorefield, C. N.; Vögtle, F. *Dendrimers and Dendrons: Concepts, Syntheses, Applications*; VCH: Weinheim, Germany, 2002. (b) Frechet, F. M. J.; Tomalia, D. A. *Dendrimers and Other Dendritic Polymers*; VCH: Weinheim, Germany, 2001.
- (6) Balzani, V.; Campagna, S.; Denti, G.; Juris, A.; Serroni, S.; Venturi, M. Designing Dendrimers Based on Transition-Metal Complexes. Light-Harvesting Properties and Predetermined Redox Patterns. *Acc. Chem. Res.* **1998**, *31*, 26–34.
- (7) Domracheva, N. E.; Morozov, V. I.; Gruzdev, M. S.; Manapov, R. A.; Pyataev, A. V.; Lattermann, G. Iron-Containing Poly(propylene imine) Dendromesogens with Photoactive Properties. *Macromol. Chem. Phys.* **2010**, *211*, 791–800.
- (8) Gutlich, P.; Goodwin, H. A. *Spin Crossover in Transition Metal Compounds (Topics in Current Chemistry)*, 1st ed.; Springer-Verlag: Berlin, Heidelberg, New York, 2004; pp 233–235.
- (9) Gutlich, P.; Hauser, A.; Spiering, H. Thermal and Optical Switching of Iron(II) Complexes. *Angew. Chem., Int. Ed. Engl.* **1994**, *33*, 2024–2054.
- (10) Linares, J.; Codjovi, E.; Garcia, Y. Pressure and Temperature Spin Crossover Sensors with Optical Detection. *Sensors* **2012**, *12*, 4479–4492.

- (11) Fujigaya, T.; Jiang, D.-L.; Aida, T. Spin-Crossover Dendrimers: Generation Number-Dependent Cooperativity for Thermal Spin Transition. *J. Am. Chem. Soc.* **2005**, *127*, 5484–5489.
- (12) Sonar, P.; Grunert, C. M.; Wie, Y.-L.; Kusz, J.; Gutlich, P.; Schluter, A. D. Iron(II) Spin Transition Complexes with Dendritic Ligands, Part I. *Eur. J. Inorg. Chem.* **2008**, *10*, 1613–1622.
- (13) Wie, Y.-L.; Sonar, P.; Grunert, M.; Kusz, J.; Schluter, D.; Gutlich, P. Iron(II) Spin-Transition Complexes with Dendritic Ligands, Part II. *Eur. J. Inorg. Chem.* **2010**, *25*, 3930–3941.
- (14) Letard, J. F.; Guionneau, P.; Goux-Capes, L. *Spin Crossover in Transition Metal Compounds (Topics in Current Chemistry)*; Springer-Verlag: Berlin, Heidelberg, New York, 2004; Vol. 235, pp 221–249.
- (15) Nihei, M.; Shiga, T.; Maeda, Y.; Oshio, H. Spin Crossover Iron(III) Complexes. *Coord. Chem. Rev.* **2007**, *251*, 2606–2621.
- (16) Koningsbruggen, P. J.; Maeda, Y.; Oshio, H. *Spin Crossover in Transition Metal Compounds (Topics in Current Chemistry)*; Springer-Verlag: Berlin, Heidelberg, New York, 2004; Vol. 233, pp 259–324.
- (17) Gruzdev, M. S.; Domracheva, N. E.; Chervonova, U. V.; Kolker, A. M.; Golubeva, A. S. Bis-Chelate Fe(III) Complex of an Azomethine at the Focal Point of a Branched Ester Functionalized with Cyclohexylbenzoic Acid. *J. Coord. Chem.* **2012**, *65*, 1812–1820.
- (18) Perdew, J. P.; Burke, K.; Ernzerhof, M. Generalized Gradient Approximation Made Simple. *Phys. Rev. Lett.* **1996**, *77*, 3865–3868.
- (19) Perdew, J. P.; Burke, K.; Ernzerhof, M. Generalized Gradient Approximation Made Simple. *Phys. Rev. Lett.* **1997**, *78*, 1396–1396.
- (20) Laikov, D. N. Ph.D. Thesis, Moscow State University, Moscow, Russia, 2000.
- (21) Laikov, D. N. *PRIRODA*, Electronic Structure Code, Version 5, 2005.
- (22) (a) Becke, A. D. Density-Functional Thermochemistry. III. The Role of Exact Exchange. *J. Chem. Phys.* **1993**, *98*, 5648–5652. (b) Stephens, P. J.; Devlin, F. J.; Chabalowski, C. F.; Frisch, M. J. Ab Initio Calculation of Vibrational Absorption and Circular Dichroism Spectra Using Density Functional Force Fields. *J. Phys. Chem.* **1994**, *98*, 11623–11627.
- (23) Neese, F. Prediction and Interpretation of the 57Fe Isomer Shift in Mössbauer Spectra by Density Functional Theory. *Inorg. Chim. Acta* **2002**, *337*, 181–192.
- (24) Schafer, A.; Horn, H.; Ahlrichs, R. Fully Optimized Contracted Gaussian Basis Sets of Triple Zeta Valence Quality for Atoms Li to Kr. *J. Chem. Phys.* **1994**, *100*, 5829–5835.
- (25) Neese, F. ORCA—an Ab Initio, Density Functional and Semiempirical Program Package, 2.8; University of Bonn: Bonn, Germany, 2011.
- (26) Conti, A. J.; Chadha, R. K.; Sena, K. M.; Rheinholt, A. L.; Hendrickson, D. N. Dynamics and Phase Transitions in Spin-Crossover Complexes: X-ray Structures and Basic Crossover Phenomena in the Solvate Series Bis(3-ethoxysalicylideneaziridinopropylaminate)iron Perchlorate Solvate. *Inorg. Chem.* **1993**, *32*, 2670–2680.
- (27) Ohshio, H.; Maeda, Y.; Takashima, Y. Rapid Electronic Relaxation Phenomenon in a ²T - ⁶A Spin-Equilibrium System. *Inorg. Chem.* **1983**, *22*, 2684–2689.
- (28) Maeda, Y.; Tsutsumi, N.; Takashima, Y. Examples of Fast and Slow Electronic Relaxation between ⁶A and ²T. *Inorg. Chem.* **1984**, *23*, 2440–2447.
- (29) Timken, M. D.; Strouse, C. E.; Soltis, S. M.; Daverio, S. A.; Hendrickson, D. N.; Abdel-Mawgoud, A. M.; Wilson, S. R. Dynamics of Spin-State Interconversion and Cooperativity for Ferric Spin-Crossover Complexes in the Solid State. 5. Variable-Temperature Spectroscopic, Magnetic, and Single-Crystal X-ray Structural Characterizations of the Spin-State and Order-Disorder Transformations of a Schiff Base Complex. *J. Am. Chem. Soc.* **1986**, *108*, 395–402.
- (30) Kennedy, B. J.; McGrath, A. C.; Murray, K. S.; Skelton, B. W. Variable-Temperature Magnetic, Spectral, and X-ray Crystallographic Studies of «Spin-Crossover» Iron(III) Schiff-Base-Lewis-Base Adducts. Influence of Noncoordinated Anions on Spin-State Interconversion Dynamics in [Fe(salen)(imd)₂]Y Species (Y =

ClO_4^- , BF_4^- , PF_6^- , BPh_4^- ; imd = Imidazole). *Inorg. Chem.* **1987**, *26*, 483–495.

(31) Mohan, M.; Gupta, N. S.; Chandra, L.; Jha, N. K.; Prasad, R. S. On the Nature of the High-Spin ($^6\text{A}_1$) - Low-Spin ($^2\text{T}_2$) Transition in $[\text{Fe}(\text{3-CH}_3\text{OSPH})_2]\text{Y}$ Complexes. *Inorg. Chim. Acta* **1988**, *141*, 185–192.

(32) Bhadbhade, M. M.; Srinivas, D. Spin Crossover in Substituted N,N'-Ethylenebis(salicylideneamine) Iron(III) Complexes: Variable Temperature EPR and X-ray Structures of $[\text{Fe}(\text{5-CH}_3\text{O-SALEN})-(\text{Im})_2]\text{Y}$, where $\text{Y}=\text{ClO}_4^-$ and Cl^- . *Polyhedron* **1998**, *17*, 2699–2711.

(33) Wickman, H. H.; Klein, M. P.; Shirley, D. A. Paramagnetic Resonance of Fe^{3+} in Polycrystalline Ferrichrome A. *J. Chem. Phys.* **1965**, *42*, 2113–2118.

(34) Aasa, R. Powder Line Shapes in the Electron Paramagnetic Resonance Spectra of HighSpin Ferric Complexes. *J. Chem. Phys.* **1970**, *52*, 3919–3931.

(35) DeSimone, R. E. Electron Paramagnetic Resonance Studies of Low-Spin d5 Complexes. Trisbidentate Complexes of Iron(III), Ruthenium(III), and Osmium(III) with Sulfur-Donor Ligands. *J. Am. Chem. Soc.* **1973**, *95*, 6238–6244.

(36) Bohan, T. L. Analysis of Low-Spin ESR Spectra of Ferric Heme Proteins: A Reexamination. *J. Magn. Reson.* **1977**, *26*, 109–118.

(37) Domracheva, N.; Pyataev, A.; Manapov, R.; Gruzdev, M.; Chervonova, U.; Kolker, A. Structural, Magnetic and Dynamic Characterization of Liquid Crystalline Iron(III) Schiff Base Complexes with Asymmetric Ligands. *Eur. J. Inorg. Chem.* **2011**, *8*, 1219–1229.

(38) Neese, F.; Solomon, E. I. Calculation of Zero-Field Splittings, g-Values, and the Relativistic Nephelauxetic Effect in Transition Metal Complexes. Application to High-Spin Ferric Complexes. *Inorg. Chem.* **1998**, *37*, 6568–6582.

(39) Murav'ev, V. I. EPR Spectra and Structures of Spin-Variable Iron(III) Complexes. *Russ. J. Coord. Chem.* **2011**, *37*, 861–867.

(40) Domracheva, N. E.; Ovchinnikov, I. V.; Turanov, A. N.; Konstantinov, V. N. EPR Detection of Presumable Magnetoelectric Interaction in the Liquid-Crystalline State of an Iron Mesogen. *J. Magn. Magn. Mater.* **2004**, *269*, 385–392.

(41) Conti, A. J.; Kaji, K.; Nagano, Y.; Sena, K. M.; Yumoto, Y.; Chadha, R. K.; Rheinhold, A. L.; Sorai, M.; Hendrickson, D. N. Dynamics and Phase Transitions in Spin-Crossover Complexes: Detailed Nature of Phase Transitions in the Solvate Series Bis(3-ethoxysalicylideneaziridinopropylamino)iron Perchlorate Solvate. *Inorg. Chem.* **1993**, *32*, 2681–2693.

(42) Ewald, A.; Martin, R. L.; Ross, I. G.; White, A. H. Anomalous Behaviour at the $^6\text{A}_1$ - $^2\text{T}_2$ Crossover in Iron (III) Complexes. *Proc. R. Soc. London, Ser. A* **1964**, *280*, 235–257.

(43) Domracheva, N.; Galyametdinov, Yu.; Ovchinnikov, I.; Zuev, Y. Dielectric and ESR Behaviour of the First Mesogenic Iron Complex: Local Ordering of Dipole Moments in the Mesophase. *Ferroelectrics* **1996**, *185*, 81–86.

(44) Mims, W. B. *The Linear Electric Field Effect in Paramagnetic Resonance*; Clarendon Press: Oxford, U.K., 1976.

(45) Bersuker, I. B. Pseudo Jahn-Teller Origin of Perovskite Multiferroics, Magnetic-Ferroelectric Crossover, and Magnetoelectric Effects: the d^0 - d^{10} Problem. *Phys. Rev. Lett.* **2012**, *108*, 137202.

(46) Summerton, A. P.; Diamantis, A. A.; Snow, M. R. The Crystal Structure of Bis[N-(2-aminoethyl)salicylaldiminato] Iron (III) Chloride Monohydrate, a Low Spin Iron(III) Complex Stabilized by Lattice Water. *Inorg. Chim. Acta* **1978**, *27*, 123–128.